A Proof of SFTD basic properties

Proposition 3. ***(SFTD Stability)*** *For any scalar functions f, f', g, g' on a grid, or on a graph vertex set:*

$$d_B(\textit{F-Cross-Barcode}_k(f,g), \textit{F-Cross-Barcode}_k(f',g')) \leq \max(\max_i|f(i)-f'(i)|, \max_i|g(i)-g'(i)|). \quad (5)$$

Here d_B denotes the bottleneck distance between persistence barcodes [13].

Proof. The proof is parallel in the simplicial and in the cubical cases. By construction, F-Cross-Barcode$_k(f,g)$, F-Cross-Barcode$_k(f',g')$ are the $k-$th persistence barcodes of the lower-star filtrations induced by the functions $\tilde{f}$, $\tilde{f'}$ on the doubled graph $\tilde{\mathcal{G}}$ from section 4.1. If $\max(\max_i|f(i)-f'(i)|, \max_i|g(i)-g'(i)|) = \varepsilon$, then $\max_{j\in\tilde{\mathcal{V}}}|\tilde{f}(j)-\tilde{f'}(j)| \leq \varepsilon$. Hence the filtration of each simplex in the lower star filtration induced by $\tilde{f}$ on $\tilde{\mathcal{G}}$ changes at most by ε under the perturbation $\tilde{f'}$. It follows from e.g. the description of metamorphoses of canonical forms in [5] that the birth or the death of each segment in the $k-$th barcode of $\tilde{\mathcal{G}}$ changes under such perturbation at most by ε.

Proposition 4. *For any scalar functions f, f':*

$$\|\textit{F-Cross-Barcode}_k(f,f')\|_B \leq \max_i|f(i)-f'(i)|.$$

Proof. Apply equation (5) with $g = g' = f'$.

Let $C^{f\leq\alpha}(\mathcal{G})$ denotes the simplicial (cubical) subcomplex of the simplicial (cubical) complex associated with graph (lattice) $\mathcal{G}$, containing all simplices (cells) on which $f \leq \alpha$. The proof of propositon 1 follows from the exactness of the sequence in equation 6 below.

Theorem 1. *F-Cross-Barcode$_k(f,g)$ has the folowing properties:*
- *if $f(i) = g(i)$ for any $i \in \mathcal{V}$, then F-Cross-Barcode$_k(f,g) = \varnothing$ for any $k \geq 0$;*
- *if $g(i) = \min_{j\in\mathcal{V}} f(j)$ for any i, then for all $k \geq 0$: F-Cross-Barcode$_{k+1}(f,g) =$ Barcode$_k(f)$ the standard barcode of the lower star filtration induced by f on graph $\mathcal{G}$;*
- *for any value of threshold α, the following sequence of natural linear maps of homology groups*

$$\xrightarrow{r_{3i+3}} H_i(C^{f\leq\alpha}(\mathcal{G})) \xrightarrow{r_{3i+2}} H_i(C^{\min(f,g)\leq\alpha}(\mathcal{G})) \xrightarrow{r_{3i+1}} \xrightarrow{r_{3i+1}} H_i(C^{\tilde{f}\leq\alpha}(\tilde{\mathcal{G}})) \xrightarrow{r_{3i}} H_{i-1}(C^{f\leq\alpha}(\mathcal{G})) \xrightarrow{r_{3i-1}} \dots$$
$$\dots \xrightarrow{r_1} H_0(C^{f\leq\alpha}(\mathcal{G})) \xrightarrow{r_0} H_0(C^{\min(f,g)\leq\alpha}(\mathcal{G})) \xrightarrow{r_{-1}} H_0(C^{\tilde{f}\leq\alpha}(\tilde{\mathcal{G}})) \xrightarrow{r_{-2}} 0 \quad (6)$$

is exact, i.e. for any j the kernel of the map r_j is the image of the map r_{j+1}.

Proof. The proof of the first two properties is immediate from the definiton of F-Cross-Barcode$_k(f,g)$. The proof of the third property follows from the proposition 5.

Proposition 5. *The embeddings of graphs* $\mathcal{G}^{f\le\alpha} \subseteq \mathcal{G}^{\min(f,g)\le\alpha} \subset \tilde{\mathcal{G}}^{\tilde{f}\le\alpha}$ *give distinguished triangles, see [18], in the homotopy category of chain complexes:*

$$C^{f\le\alpha}(\mathcal{G}) \to C^{\min(f,g)\le\alpha}(\mathcal{G}) \to C^{\tilde{f}\le\alpha}(\tilde{\mathcal{G}}) \to C^{f\le\alpha}(\mathcal{G})[-1]. \tag{7}$$

Proof. The proof is parallel to the proof of proposition A.3 from [7].

B Connection to Representation Topology Divergence

Representation Topology Divergence (RTD) [7] is a tool to compare two representations R_1, R_2 of some set of objects $\mathcal{V}$. RTD measures the dissimilarity in multi-scale topology between two point clouds of equal size with a one-to-one correspondence. Here we establish connections between SFTD and RTD and highlight differences.

A unified view of SFTD and RTD involves two elements:

1. calculating a persistence barcode of a filtered simplicial complex derived from the double graph $\tilde{\mathcal{G}}$, see Fig. 2a;
2. usage of a specific filtration function $T : \mathcal{C}(\tilde{\mathcal{G}}) \to \mathbb{R}$.

Theoretically, the only restriction for T is that $T(C_1) \le T(C_2)$ when $C_1 \subseteq C_2$. For SFTD, the filtration function T is defined in vertices by a vertex function $\tilde{f}$ (see Section 4) and extended to the rest of simplices by a formula $T(C) = \max_{v\in C} \tilde{f}(v)$. While for RTD, $T(C)$ conforms to the Vietoris-Rips filtration with distance-like weights and is defined on vertices and edges as follows:

$$\begin{gathered} T(A_i) = T(A_j) = T(O) = 0 \\ T(A'_i, A'_j) = \min(\mathrm{dist}(R_1(i), R_1(j)), \mathrm{dist}(R_2(i), R_2(j))), \\ T(A_i, A'_j) = T(A_i, A_j) = \mathrm{dist}(R_1(i), R_1(j)), \\ T(A_i, A'_i) = T(O, A_i) = 0. \end{gathered}$$

Here, for two objects $i, j \in \mathcal{V}$ we have their representations $R_1(i), R_2(i)$ and a distance function $\mathrm{dist}(R_1(i), R_2(i))$. For the rest of the simplices, the filtration function is extended by a formula $T(C) = \max_{v_1,v_2\in C,(v_1,v_2)\in\tilde{\mathcal{E}}} T((v_1, v_2))$.

C Computational complexity of SFTD

The dominating step in SFTD computation is an evaluation of a persistence barcode. Generally, it is at worst cubic in the number of cubes/simplexes involved. In practice, the computation is faster since the boundary matrix is typically sparse for real datasets. SFTD for 512^2 or 64^3 lattices can be calculated in seconds.

D Details on the experiment with SHAPR

For experiments, we used the official repository[9]. We closely followed the official pipeline and trained with the loss: $\mathcal{L}_{SHAPR} + \lambda \cdot SFTD$, where λ was selected from the set $\{1.0, 0.5, 0.25, 0.125, 0.06\}$ by Dice error on cross-validation. For baselines (SHAPR, SHAPR+W.D.) we used predictions from a zip-archive from the official repository.

E Details on the experiment with 3D segmentation

For experiments, we used the repository [10] with the implementation of Swin UNETR model pretrained on BraTS21 dataset of the MONAI Project framework [11]. The ground truth and predicted segmentations have three channels corresponding to NCR, ED, ET parts of tumor. In the experiments, we analyze and visualize the segmentations corresponding to each channel separately. To visualize the distinctive topological features provided by F-Cross-Barcode, we separately compute SFTD between ground truth and predicted segmentations and vice versa. Topological features provided by SFTD between the ground truth and prediction are depicted in the ground truth segmentation while SFTD between the prediction and ground truth are depicted in the predicted segmentation. In each example, the object's voxels have values of 1 while the background's voxels have values of 0. In the visualizations of the persistence barcodes and F-Cross-Barcodes, we omit the infinite half-line in H_0 for the ease of perception.

F Additional results for 3D segmentation

In this section, we provide additional examples of topological errors between the ground truth and predicted 3D segmentations, see Figures 12, 13. The predicted segmentations in figures 12b, 13b have incorrect localization of clusters compared to the ground truth in figures 12a, 13a. In both cases, this difference is indistinguishable by persistence barcodes (see figures 12c, 12d, 13c, 13d) but is revealed by the F-Cross-Barcodes (see figures 12e, 13e).

G Additional experiments for 2D segmentation

In 2D segmentation, optimizing loss functions based on pixel-overlap is often insufficient to capture the correct topology of segmented objects. Betti matching [32] is a topological metric and loss function for supervised image segmentation. When used as a loss function, Betti matching improves topological performance of segmentation models while preserving the volumetric quality.

[9] `https://github.com/marrlab/SHAPR_torch`

[10] `https://github.com/Project-MONAI/research-contributions/tree/main/SwinUNETR/BRATS21`

[11] `https://github.com/Project-MONAI`

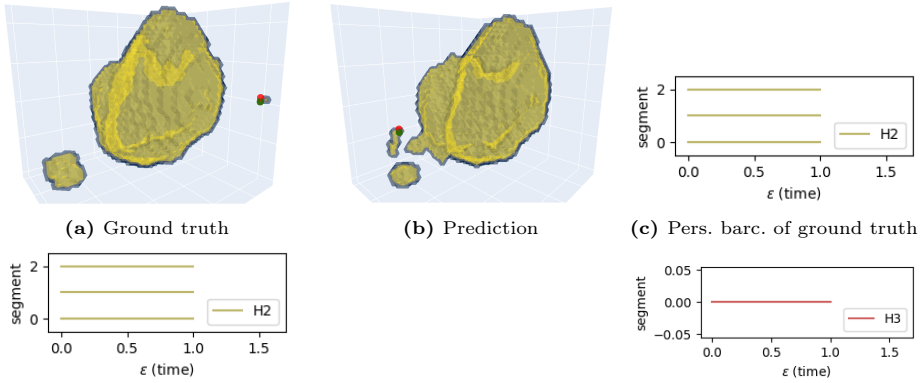

(a) Ground truth **(b)** Prediction **(c)** Pers. barc. of ground truth

(d) Pers. barc. of prediction **(e)** F-Cross-Barcode

Fig. 12: Examples of topological errors in 3D segmentation. Predicted segmentation (b) has incorrect localization of one cluster compared to the ground truth (a). This difference is indistinguishable by persistence barcodes (c), (d) but is revealed by F-Cross-Barcode (e).

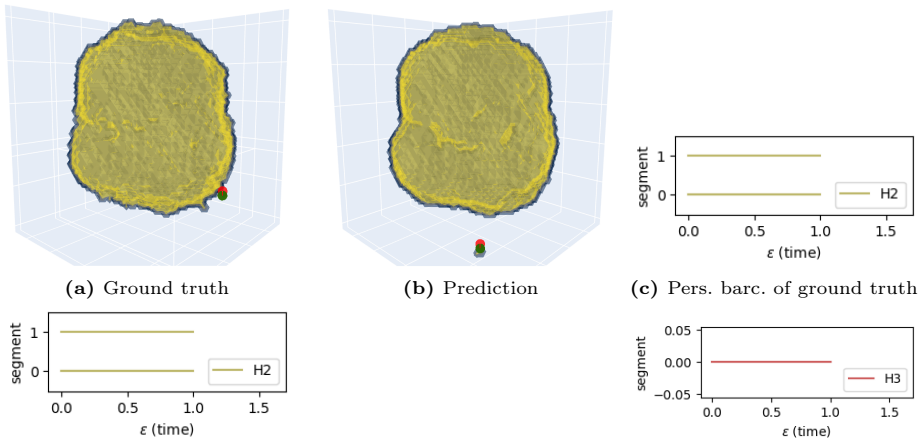

(a) Ground truth **(b)** Prediction **(c)** Pers. barc. of ground truth

(d) Pers. barc. of prediction **(e)** F-Cross-Barcode

Fig. 13: Examples of topological errors in 3D segmentation. The ground truth segmentation (a) has a tiny cluster that is incorrectly predicted by the model (b). This difference is indistinguishable by persistence barcodes (c), (d) but is revealed by F-Cross-Barcode (e).

We strictly followed the experimental setup from [32] to compare SFTD with Betti matching loss on CREMI [17] and colon cancer cell (Colon) [10] datasets. We replaced the topological loss term in Betti matching with SFTD with $p = 2$ in up to 2 dimensions. Table 3 provides experimental results. Our method has similar segmentation quality (Dice, clDice, accuracy) and lower topological errors (τ^{err}, β^{err}) - up to 35%. Also, evaluation of SFTD loss is ~ 35 times faster than Betti matching loss.

Table 3: Errors of 2D segmentation for CREMI and Colon datasets.

Method	Dice ↑	clDice ↑	Acc. ↑	τ^{ERR} ↓	β^{ERR} ↓
CREMI dataset [17]					
Betti matching [32]	0.893	0.941	0.959	129.80	79.16
SFTD	0.885	0.941	0.955	126.48	62.64
Colon dataset [10]					
Betti matching [32]	0.907	0.871	0.975	32.00	21.50
SFTD	0.901	0.889	0.971	21.50	14.00